Available online at www.sciencedirect.com
ScienceDirect
Catalysis Today 117 (2006) 475–483
CATALYSIS TODAY
www.elsevier.com/locate/cattod

Fuel-rich methane combustion: Role of the Pt dispersion and oxygen mobility in a fluorite-like complex oxide support

V.A. Sadykov [a,*], T.G. Kuznetsova [a], Yu.V. Frolova-Borchert [a], G.M. Alikina [a], A.I. Lukashevich [a], V.A. Rogov [a], V.S. Muzykantov [a], L.G. Pinaeva [a], E.M. Sadovskaya [a], Yu.A. Ivanova [a], E.A. Paukshtis [a], N.V. Mezentseva [a], L.Ch. Batuev [a], V.N. Parmon [a], S. Neophytides [b], E. Kemnitz [c], K. Scheurell [c], C. Mirodatos [d], A.C. van Veen [d]

[a] *Boreskov Institute of Catalysis SB RAS, pr. Lavrentieva, 5, Novosibirsk 630090, Russia*
[b] *Institute of Chemical Engineering and High-Temperature Processes, Patras, Greece*
[c] *Institute for Chemistry, Humboldt-University, Berlin, Germany*
[d] *Institut de Recherches sur la Catalyse, Villeurbanne, France*

Available online 20 July 2006

Abstract

For catalysts comprised of Pt supported onto dispersed complex fluorite-like oxides (ceria doped by Pr, Gd, Sm, or CeO_2–ZrO_2 doped by La, Gd or Pr), the effects of the oxygen mobility in supports and Pt dispersion on the performance in methane selective oxidation into syngas at short contact times were elucidated using combination of kinetic and spectroscopic methods. While in general any simple universal relation between the oxygen mobility, Pt dispersion and the rate of methane transformation into syngas was not found, for some series, a good correlation was observed agreeing with the bifunctional scheme of the methane selective oxidation into syngas.

Keywords: Syngas; Methane; Fuel-rich combustion; Pt; Fluorite-like supports; Lattice oxygen mobility and reactivity; Isotope exchange; TPR; SSITKA; Transients; Mechanism

1. Introduction

Catalysts comprised of doped ceria, zirconia or ceria–zirconia oxides with supported Pt were recently shown to be very efficient and stable in the fuel-rich hydrocarbons combustion ensuring a high yield of syngas at short contact times [1,2]. This makes them promising for replacing expensive Rh/corundum foam catalysts first suggested for this application [3].

The role of Pt as the active component is mainly considered to be activation of the hydrocarbon molecule by the homolytic cleavage of the C–H bond thus generating hydrogen atoms and hydrocarbon fragments adsorbed on the metal particles [3,4]. The carbon build-up leading to coking and loss of activity is prevented due to rapid interaction of those fragments with the oxygen atoms supplied to the metal particle-oxide support perimeter via the surface diffusion thus generating CO and hydrogen [5]. Complex ceria-containing fluorite-like oxides (possessing required surface lattice oxygen mobility and reactivity along with the phase stability in strongly reducing conditions) appear to be the most promising oxide supports [1,2,6]. Incorporation of low-valence cations into the lattice of ceria or ceria–zirconia solutions is expected to create anion vacancies, thus improving the lattice oxygen mobility [7]. However, up to date, systematic studies of the effect of a dopant type and its content on the lattice oxygen mobility and surface properties of dispersed fluorite-like solid solutions are missing. Furthermore, no straightforward correlations have been obtained relating oxide properties with the performance of supported platinum group metals in the transformation of methane into syngas. Recent results of Wei and Iglesia [8–10] even suggest the absence of any bifunctional CH_4 reforming pathways for Pt group metals and Ni on such supports as ZrO_2,

* Corresponding author. Tel.: +7 383 3308763; fax: +7 383 3308056.
E-mail address: sadykov@catalysis.nsk.su (V.A. Sadykov).

0920-5861/$ – see front matter © 2006 Elsevier B.V. All rights reserved.
doi:10.1016/j.cattod.2006.06.017

γ-Al_2O_3, CeO_2–ZrO_2 (Zr/Ce = 4), MgO. This is explained by a kinetic scheme in which only C–H bond activation has kinetic relevance, while other steps occur much faster.

Some arguments in favor of the bifunctional scheme of methane fuel-rich combustion/partial oxidation (POM) can be obtained by comparing the specific rate of POM for catalysts with a close Pt dispersion but broadly varying surface/bulk oxygen mobility. This mobility can be estimated by dynamic methods either for standard oxidized state of samples (oxygen isotope exchange, temperature-programmed oxygen desorption) or for their partially reduced state (H_2 or CH_4 TPR). However, for proving the bi-functional scheme, estimation of the rate of the oxygen-containing species transfer between the Pt particles and the support in the course of catalytic reaction would be of crucial importance. This can be made by using kinetic transients, where relaxation curves fitting allows to estimate the rate constants of corresponding steps [11,12].

In the frame of this bi-functional scheme, another important factor is the Pt dispersion. This parameter determines both Pt efficiency in the C–H bond cleavage in methane molecule [8] as well as resulting flux of oxygen-containing species to the boundary between Pt clusters and support. IR spectroscopy of adsorbed CO test molecule sensitive not only to the number of accessible Pt sites, but to their clustering degree and charge state as well [13,14] can be applied for this purpose.

This work summarizes results of systematic studies of the role of the oxygen mobility in support, Pt dispersion and Pt-support interaction for ceria and ceria–zirconia systems doped with La, Sm, Pr or Gd and promoted with Pt as catalysts of POM. Detailed characterization of the samples real structure and surface properties has already been presented in a number of publications [14–25] and will be considered here only in the extent required to clarify the factors determining mobility/reactivity of the oxygen and catalytic activity in the reaction of methane selective oxidation into syngas.

2. Experimental

Samples of complex oxides including ceria doped with Gd, Sm, or Pr ($Ce_{1-x}Me_xO_{2-y}$, Me content x = 0–0.5) and $Ce_{0.5-x/2}Zr_{0.5-x/2}$ Me_xO_{2-y} (Me = La, Gd or Pr, x = 0–0.3) were prepared via the polymerized precursor (Pechini) route [1] with modifications of procedures described earlier [14,15,23,24] and calcined at 500–700 °C. All samples were nanocrystalline fluorite-like solid solutions, excluding La-doped ceria–zirconia system at xLa ≥ 0.2 comprised of two fluorite-like phases [15]. Pt (1.4 wt.%) was supported by the incipient wetness impregnation with H_2PtCl_6 solution followed by drying and calcination at 500 °C.

The surface features of samples (support sites and state of supported Pt) were characterized by Fourier transform infra-red spectroscopy (FTIRS) of CO or O_2^- test species adsorbed at 77 K using a Shimadzu 8300 spectrometer and earlier described procedures [14,24].

BET specific surface area of samples (varied in the range of 35–150 m^2/g) was determined from the Ar thermal desorption data.

A dynamic ^{18}O-isotope exchange experiments in the temperature-programmed mode were carried out in the static installation with on-line-coupled quadruple mass spectrometer QMG421 I (Pfeiffer Vacuum GmbH) [26,27]. To characterize the oxygen mobility by using data obtained in the temperature-programmed mode, a dynamic degree of exchange normalized to the surface area of a sample was used [18,21,26]:

$X_s = \lambda_s\{(\alpha^0/\alpha) - 1\}$, where $\lambda_s = N/N_s$ (monolayers), N is the number of O atoms in the gas phase; N_s is the number of exchangeable oxygen atoms in the monolayer of an oxide, α^0, α are initial and current fraction of ^{18}O in the gas phase.

Experiments in the temperature-programmed mode for O_2 TPD, H_2 TPR, and partial oxidation of CH_4 were carried out in a flow quartz reactor using a kinetic installation equipped with GC, an on-line IR absorbance gas analyzer PEM-2M, TCD, an electrochemical sensor for O_2 and a polarographic sensor for H_2 monitoring with the data acquisition and processing through a PC as described in details elsewhere [16–24].

For the sample of Ce–Zr–La–O series containing 20% La, both with Pt and without it, steady-state isotopic transient kinetic analysis (SSITKA) experiments were carried out as well in the temperature range 650–850 °C. When the steady state was achieved under 2% $^{16}O_2$ in Ar flow, it was replaced stepwise by the same one containing $^{18}O_2$, the transient changes in the gas isotopic composition being continuously monitored by a VG-Gas Lab mass-spectrometer.

In relaxation experiments, 0.05 g of a catalyst was loaded into a tubular quartz reactor (L = 300 mm, i.d. = 3 mm) and heated up to 650 °C under flowing He. Prior to every experiment, a sample was oxidized in 2.2% O_2 + He flow (flow rate 5 ml/s) for 30 min. Reduction of a sample was carried out by contacting sample with a pure H_2 flow for 0.5 h at the same temperature. Before reaction mixture feeding, O_2 or H_2 were flushed by He purging for 2 min. Switches from He to reaction mixture and vice versa (flow rates were 5 ml/s for both mixtures) were performed with continuous monitoring of the gas phase composition by a QMS-200 (SRC) mass spectrometer and on-line chromatographic analysis. Reaction mixtures of 4.6% CH_4 (+2.2% O_2) in He were used in these switches.

3. Results and discussion

3.1. Catalytic activity in POM

Fig. 1 compares the specific rates of CH_4 consumption, H_2 and CO_2 generation for all studied series of samples estimated using the efficient first-order rate equation for the plug-flow reactor satisfactorily describing the experimental data [19,20,22]. A broad (by more than one order of magnitude) variation of these rates at the same Pt content and its comparable dispersion (vide infra) is quite clear, suggesting a structural sensitivity of this reaction. For all systems, catalysts performance both in model and realistic [20] feeds was stable, and no coking of catalysts was observed. Obviously, the support effect on the catalytic activity of Pt in POM is prominent, and support oxygen mobility could be among decisive factors. Hence, subsequent analysis is directed to elucidation of

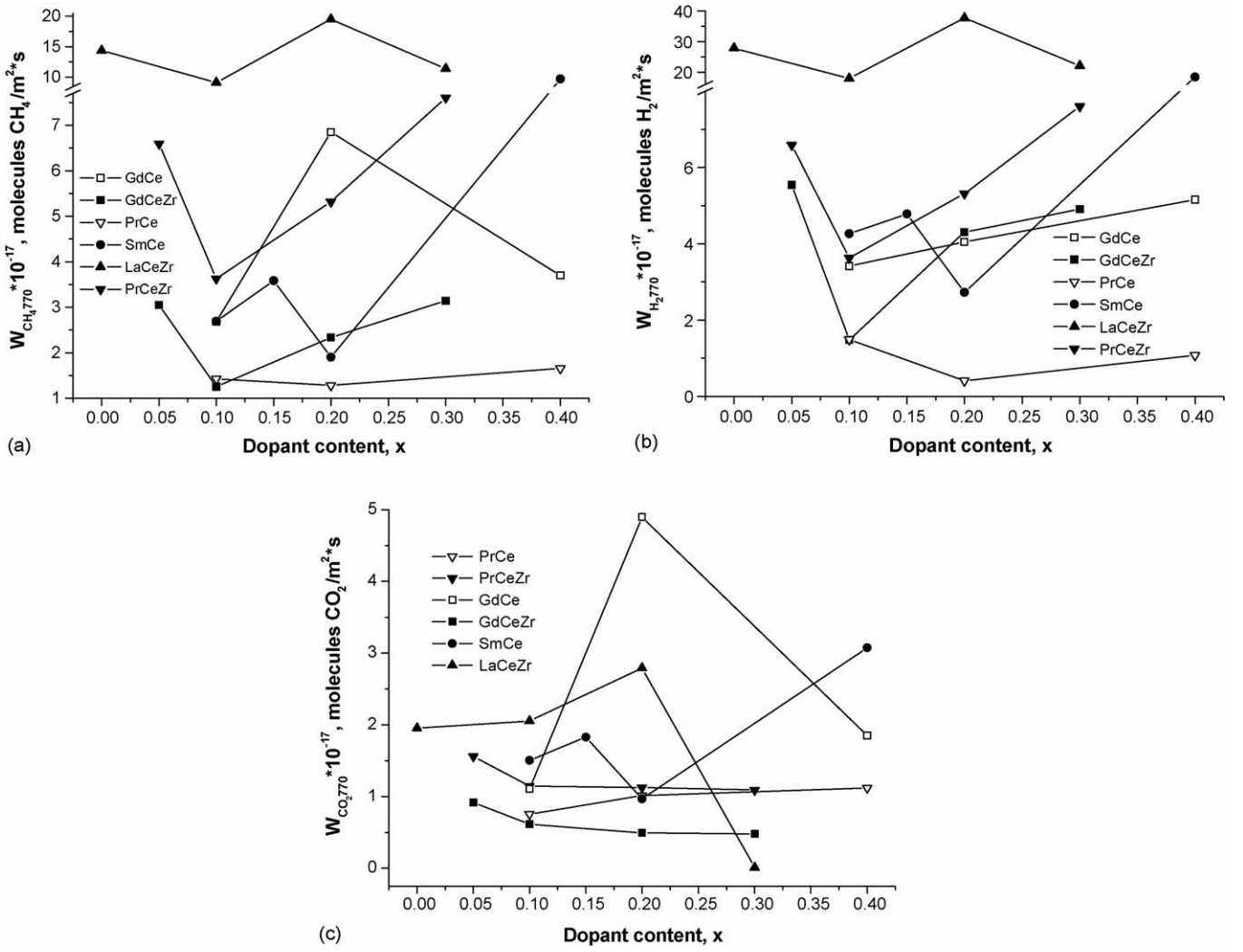

Fig. 1. Specific rates of methane conversion (a) and products formation ((b) H_2, (c) CO_2) in methane selective oxidation vs. dopant content in Pt-supported doped ceria or ceria–zirconia systems. 1% CH_4 + 0.5% O_2 in He, 770 °C, 5 ms contact time, temperature-programmed mode, samples pretreated in 10% O_2 in He at 500 °C before reaction.

relations (if any) between properties of supports and catalytic activity of Pt-supported samples in POM with a due regard for the Pt-support interaction and Pt dispersion.

3.2. Oxygen mobility and state of supported Pt in oxidized samples

3.2.1. Dynamic isotope exchange

For all studied systems, only the third type of exchange with participation of two oxygen atoms of support was observed [14,18,21].

Fig. 2 compares the dynamic degree of exchange for series of Gd or Pr-doped ceria samples. For Gd-doped ceria, the lattice oxygen mobility goes through the maximum at xGd = 0.2, apparently being determined by the density of free anion vacancies [7,16,20]. At a higher doping level, clustering of vacancies and dopant cations decreases the lattice oxygen mobility [16,17]. Moreover, segregation of doping cations to the ceria surface rearranges its structure decreasing the density of surface anion vacancies and associated coordinatively unsaturated Ce^{4+} sites involved into activation of molecular oxygen species [23,24]. Similarly, for Sm-doped ceria the dynamic degree of exchange reaches a maximum at xSm = 0.2, while being practically identical at x = 0.1 and 0.4 [14].

For Pr-doped ceria, the dynamic degree of exchange increases with the doping level reflecting the increase in the concentration of $Pr^{3+/4+}$ in the lattice [17]. As the result, at the highest dopant content, the dynamic degree of exchange for Pr-doped ceria is even higher than that for Gd-doped ceria apparently reflecting a higher density of free anion vacancies.

At a moderate (20 at.%) doping level, the lattice oxygen mobility is higher for Gd-doped ceria as compared with other two systems [16]. This is explained by the highest density of free anion vacancies for this system generated due to substitution of Ce^{4+} by Me^{3+} cations. Since the Pr cation is present in the ceria lattice simultaneously in Pr^{3+} and Pr^{4+} states [17], at the same dopant content, the density of anion vacancies is apparently lower for Pr-doped ceria. Since Sm^{3+} cation has a bigger radius than Gd^{3+} cation, this causes a stronger deformation of ceria lattice leading to a higher degree of clustering between anion

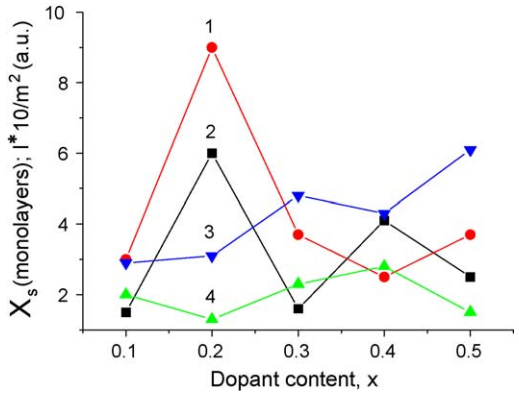

Fig. 2. The dynamic degree of the oxygen exchange (X_s) at 700 °C (1,3) and normalized intensity (I) of Pt^{2+}–CO band (2,4) for Gd (1,2) or Pr (3,4) doped ceria vs. dopant content (x) in $Ce_{1-x}Me_xO_{2-y}$, (1,3) and $Pt/Ce_{1-x}Me_xO_{2-y}$ (2,4) samples [18,21].

vacancies and a dopant decreasing the density of free anion vacancies controlling lattice oxygen mobility [16].

For ceria–zirconia system doped with Gd, La, or Pr cations, in general, the oxygen mobility (Fig. 3) is lower than that for doped ceria samples (Fig. 2), as confirmed by the isothermal isotope exchange experiments [14,20]. Since the amount of easily exchanged oxygen is below a monolayer, this oxygen appears to be mainly located in the surface layer or in the vicinity of disordered domain boundaries of these nanocrystalline systems. For nanocrystalline ceria–zirconia-based complex oxides, the lattice oxygen mobility is at present considered to be controlled not by the density of free anion vacancies (as for doped ceria systems) but by more complex Frenkel-type defects comprised of oxygen vacancy associated with oxygen in the interstitial position [28–30]. Similar defects control oxygen mobility in complex pyrochlore-type oxides [31]. A metastable κ-$Ce_2Zr_2O_8$ phase produced by soft reoxidation of reduced $Ce_2Zr_2O_7$ phase with the pyrochlore-type structure was indeed shown to possess the highest lattice oxygen mobility [32]. Since ceria–zirconia samples produced by Pechini route were obtained by decomposition of polyester resin in rather reducing conditions favorable for stabilization of Ce^{3+} cations [15], they

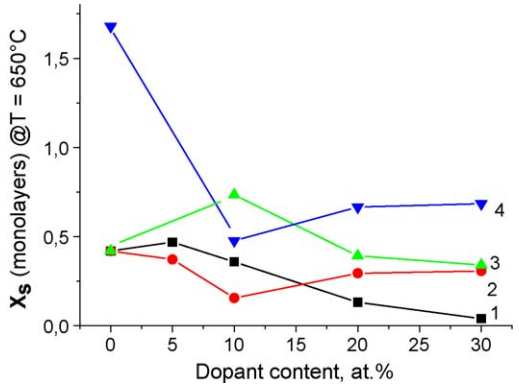

Fig. 3. The dynamic degree of the oxygen exchange (X_s) at 650 °C vs. the dopant content (mole fraction, x) for ceria–zirconia (1:1) oxide systems doped with Gd (1), Pr(2) or La(3). A 4-Pt/Ce–Zr–La–O system.

could retain in their structure pyrochlore—like fragments similar to those in the κ-$Ce_2Zr_2O_8$ phase.

The most mobile near-surface oxygen is revealed for Ce–Zr–La–O system (Fig. 3), which correlates with the biggest size of La cation, and, hence, the biggest lattice parameter of these fluorite-like oxides [15,25]. For such complex ceria–zirconia based oxides as well as pyrochlore-like solid oxide electrolytes, the increase of the lattice parameter is known to increase the size of channels for the oxygen migration, thus increasing the lattice oxygen mobility [32–34].

For ceria–zirconia systems doped with Gd^{3+} or La^{3+} cations, the increase of mobility at a low doping level is followed by its decline (Fig. 3). This suggests a complex rearrangement of the coordination polyhedra in ceria–zirconia solid solution due to doping, which could not be described by a simple model of anion vacancies generation [25]. Indeed, the increase of these dopants content is accompanied by decline of absorption in the visible range [20], which can be explained by the decrease of the content of Ce^{3+} cations and anion vacancies/oxygen interstitials in their coordination sphere responsible for the lattice oxygen mobility.

For Pr-doped ceria–zirconia, the lattice mobility first decreases (up to xPr = 0.1) then increases with the doping (Fig. 3). This phenomenon can be tentatively ascribed to the effect of redox Pr^{3+}/Pr^{4+} couple ensuring a mixed ionic–electronic conductivity in the complex oxide when a high doping level is achieved. Segregation of Pr cations at the surface or within domain boundaries [18,23] could be important in this respect.

3.2.2. *Pt dispersion and effect of Pt supporting on the oxygen mobility in oxidized samples*

In oxidized Pt/Ce–Zr–La samples, only small (0.5–1 nm) Pt clusters were revealed by TEM and XRD [14,20]. For Pt-supported doped ceria samples with a high (>20 at.%) dopant content, metallic Pt is not observed at all either by XRD [14,20] or XPS [23,24]. Hence, oxidic forms of Pt dominate for oxidized samples.

IR Spectroscopy of CO adsorbed at 77 K as test molecule revealed bands at 2158–2168 cm^{-1} (Ce^{4+}–CO complexes), 2110–2114 cm^{-1} (Me^{3+}–CO complexes), 2173–2176 cm^{-1} (Pt^{2+}–CO complexes), 2125–2132 cm^{-1} (Pt^{+}–CO complexes) and 2041–2046 cm^{-1} (Pt^{0}–CO complexes) [18,20,21,23–25]. For samples based upon doped ceria–zirconia supports, bands corresponding to Zr^{4+}–CO complexes at 2175–2180 cm^{-1} are observed as well [14,15,20]. Due to a different bonding strength and, hence, thermal stability of these complexes, and dependence of their bands intensity on CO coverage, bands corresponding to various complexes can be separated and their intensity estimated [18,20,21,23,24].

For Pt supported onto Gd-doped ceria samples, the intensity of bands corresponding to different Pt species, especially Pt^{2+}, goes through the maximum at a dopant content 20 at.%, where the highest lattice oxygen mobility is achieved (Fig. 2). A similar correlation between Pt dispersion and oxygen mobility in the bare support is observed for Pt on Pr-doped ceria (Fig. 2). This trend is explained by anchoring of Pt on the coordinatively

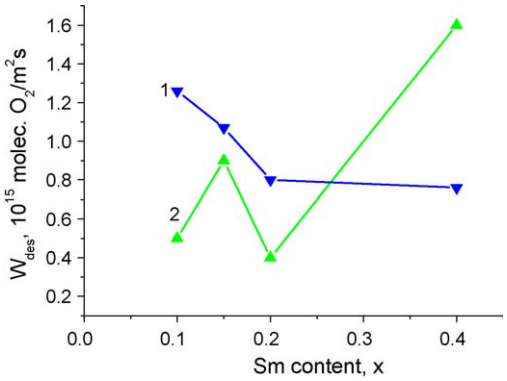

Fig. 4. Effect of Sm content (mole fraction, x) in ceria–samaria system on the maximum rates of oxygen desorption in O_2 TPD peaks at ~670 °C for the supports (1) and Pt-loaded (2) samples.

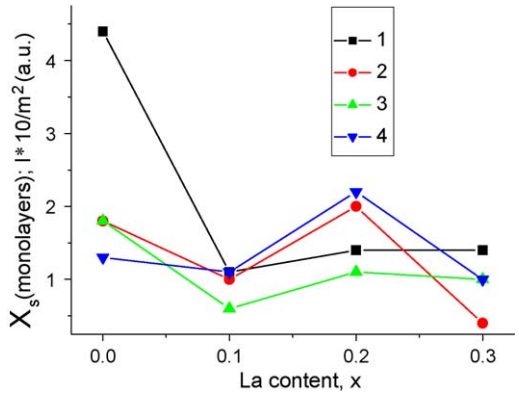

Fig. 5. The dynamic degree of the oxygen exchange (X_s) at 700 °C (1); amount of O_2 desorbed up to 900 °C (2) and normalized intensity (I) of Pt^{2+}–O_2^- (3) and Pt^{2+}–CO (4) bands for Pt/Ce–Zr–La–O system vs. La content (mole fraction, x).

unsaturated surface sites associated with the oxygen vacancies. However, at the highest Me^{3+} content, dopant dissolution in acidic H_2PtCl_6 solution results in decoration of Pt clusters by MeO_x oxidic species [7] and/or Pt cations incorporation into domain boundaries [20], decreasing the intensity of all Pt carbonyl bands [14]. However, this decline in Pt^{2+}–CO band intensity at the highest content of Gd or Pr is accompanied by an increase and not decrease of the oxygen mobility (Fig. 2).

This effect is especially pronounced for Sm-doped ceria [14,20]. While for pure supports the maximum rate of O_2 desorption in a peak situated at ~640–670 °C decreases with Sm content (Fig. 4) reflecting rearrangement of the structure leading to disappearance of free anion vacancies, for Pt-supported samples the highest rate of the oxygen desorption in the middle-temperature peak (700–780 °C) was revealed for the heavily doped sample with the lowest intensity of Pt-carbonyl bands [14]. Moreover, for this sample, the maximum rate of oxygen desorption greatly exceeds that for support (Fig. 4), while for samples with a lower dopant content, the rate of desorption decreases due to Pt supporting. A similar promoting effect of incorporated Pt for heavily doped sample was also revealed for the oxygen desorption in the isothermal part of the TPD run at 900 °C, which is apparently controlled by the oxygen diffusion from the bulk of particles to their surface along domain boundaries [14,21]. Hence, a positive effect of a strong interaction between Pt and support on the oxygen mobility is indeed observed for samples with a high content of a dopant.

In a similar way, for La-doped ceria–zirconia, the lattice oxygen mobility changes due to Pt supporting (Fig. 3). In this case, a strong positive effect is also observed for samples with a high content of La (biphasic samples), while the negative effect is revealed for the sample with a low dopant content. Hence, Pt^{2+} cations appear to be located at coordinatively unsaturated surface sites situated at outlets of domain/interphase boundaries. The additional feature revealed for this system is that Pt supporting onto undoped ceria–zirconia sample strongly increases the oxygen mobility as well. For this Ce–Zr–La–O system (Fig. 5), the amount of oxygen desorbed up to 900 °C, the dynamic degree of exchange and the intensity of Pt^{2+}–CO band correlate rather good. Pt supporting increases the amount of desorbed oxygen from 0.2 to 1 monolayer to values exceeding a monolayer (Fig. 5), which can be explained by Pt incorporation into the surface layer/domain boundaries [14,23,24]. Extensive parallels between the dynamic degree of the oxygen exchange and the band intensity corresponding to Pt^{2+} superoxide complexes (Pt^{2+}–O_2^-) observed for this system agree with the suggestion of a primary activation of molecular oxygen on these sites, at least at moderate temperatures of exchange [35]. A high intensity of such a band for Pt-supported ceria–zirconia sample without La implies that a plenty of sites exist on the surface of this support able to fix Pt as coordinatively unsaturated Pt^{2+} cations as well as small Pt^0 clusters [14]. This can be explained by nanocrystallinity of this ceria–zirconia sample [20] and a high concentration of defects including anion vacancies/oxygen interstitials, especially in vicinity of disordered domain boundaries [29]. The decrease in the intensity of Pt^{2+}–O_2^- and Pt^{2+}–CO bands with addition of 10% La to ceria–zirconia system (Fig. 5) apparently correlates with the decrease of the concentration of anion vacancies in coordination sphere of Ce cations revealed by UV–vis spectra [20] (vide supra).

Among all studied supports, the highest concentration of cationic Pt species was found for Gd-doped ceria supports followed by Pr-doped ceria [18,21]. For these systems, at a dopant content exceeding 20 at.%, Pt^0 species were not revealed at all both by FTIRS of adsorbed CO and XPS [18,21,23,24]. This agrees well with the known ability of ceria and other rare-earth oxides to stabilize oxidic forms of Pt [36,37]. For doped ceria–zirconia supports, this ability is apparently weaker since Pt^0 species were observed at any content of a dopant [20,25]. The highest concentration of Pt^{2+} species was revealed for La-doped samples, while in average it is approximately twice as low for Pt on Gd- or Pr-doped ceria–zirconia supports. For the case of these two systems, the intensity of Pt^{2+}–CO band is very close reaching a minimum at 10 at.% dopant content [25], which agrees with the same trend for Pt/Ce–Zr–La system (Fig. 5). At a dopant content >10 at.%, the intensity of Pt^{2+}–CO band increases for Gd- or Pr-doped samples up to same value as for La-doped system at 30 at.% doping level.

3.3. Surface/bulk oxygen reactivity and mobility under reducing conditions

In the H_2 TPR runs up to 800 °C, up to two monolayers of oxygen are removed from the Pt-supported samples exceeding by far the amount required to reduce all present cationic Pt species. Hence, these peaks with T_{max} situated in the range of 220–290 °C as dependent upon the support type, certainly correspond to the bulk (or, at least, near-surface) reduction of the complex oxide, their intensity (maximum or ''peak'' rate) being determined by the lattice oxygen mobility [14,18,20,21]. On the other hand, the amount of oxygen removed in these peaks is still much lower than that corresponding to complete reduction of doped ceria sample, hence, the oxide stoichiometry is expected to be rather close to that under POM reaction conditions.

Higher values of ''peak'' reduction rates for Pt-promoted Ce–Zr–La–O system as compared with ceria–zirconia systems doped by Gd or Pr (Fig. 6) agree with a higher lattice oxygen mobility for the former system estimated by the isotope exchange (vide supra). For Pt/Ce–Zr–La–O samples, H_2 TPR peaks are situated at lower (~220–240 °C) temperatures as compared with those for Pt/Gd(Pr)-doped ceria (~250 °C) [18,20,21,23,24]. This suggests a higher efficiency of H_2 dissociation on Pt clusters fixed at Ce–Zr (La) complex oxides and, hence, a higher flux of H atoms to the support sustaining the high rate of oxides reduction by hydrogen [7]. This correlates with a more oxidized state of Pt on doped ceria supports (vide supra) decreasing its ability for the homolytic rupture of H–H as well as C–H bonds [38].

For Pt/Gd(Pr)-doped ceria–zirconia samples, H_2 TPR ''peak'' rates vary with a doping level in a different manner reflecting mainly mobility of the lattice oxygen. For Pr-doped ceria–zirconia system, the downward shift of the T_{max} from ~285 to ~265 °C and increase of the ''peak'' rate with the Pr content (Fig. 6) were observed. These features could be tentatively assigned to the increase of mixed ionic–electronic conductivity of this system with Pr content (effect of conducting $Pr^{3+/4+}$ chains in the lattice or within domain boundaries) facilitating the oxygen mobility, though variation of the Pt dispersion could be important as well. For Gd-doped ceria–zirconia, the trend in the maximum rate variation with the dopant content is similar to that of La-doped ceria–zirconia (Fig. 6). Hence, similar factors could control these rates including variation of the Pt dispersion, incorporation of Pt into domain boundaries, variation of samples defect structure and segregation of a dopant on the surface [20].

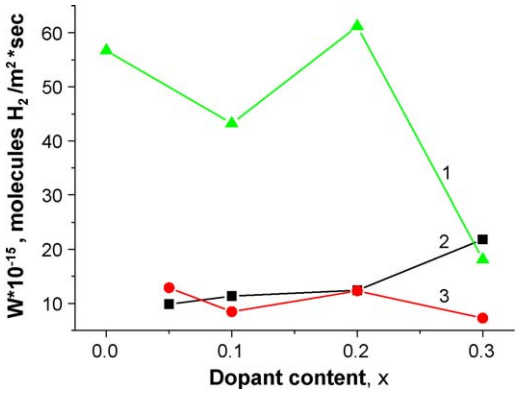

Fig. 6. Effect of the type and content of dopant (mole fraction, x) on the maximum rates of H_2 TPR in Pt/ceria–zirconia-based samples doped with La (1), Pr (2) and Gd (3).

3.4. Catalytic activity versus Pt dispersion and oxygen mobility

A comparison of the catalytic activity of studied systems in the reaction of methane selective oxidation into syngas (Fig. 1) with the Pt dispersion estimated by the intensity of Pt^{2+} carbonyl bands (Figs. 2 and 5) and the oxygen mobility and reactivity (Figs. 2–6) revealed absence of any universal correlations between these characteristics valid for all systems. This can be explained by variation of the ability of supported Pt to activate methane as well as the reactive oxygen bonding strength determining syngas selectivity.

For a given system, such as Pt/Ce–Zr–La–O, the specific rates of methane transformation and syngas (H_2) formation at short contact times (Fig. 1) correlate with the lattice oxygen mobility and Pt dispersion estimated by the intensity of Pt^{2+}–CO band (Fig. 5). In contrary, no correlations were found between activity and intensity of Pt^0–CO or Pt^+–CO bands (2050–2130 cm^{-1} range) [20]. This suggests that small Pt clusters formed from Pt^{2+} cations under the influence of the reaction mixture are the most reactive sites for CH_4 dissociation, while the efficient oxygen transfer from the support to these clusters prevents their coking by transforming CH_x fragments into CO and H_2. The non-linear trend in the variation of Pt^{2+} cations concentration and near-surface/lattice oxygen mobility with the La content is explained by the interplay of several factors including a decline of the density of point defects—anion vacancies due to the lattice rearrangement, increase in the density of domain/interphase boundaries at xLa = 0.2 due to decomposition of homogeneous fluorite-like oxide solid solution into two phases and segregation of La on the surface/domain boundaries favoring Pt incorporation into the subsurface layer/domain boundaries and decoration of Pt clusters by LaO_x fragments [20]. For this system, the rate of deep oxidation products (CO_2) formation is much lower than that of H_2 (Fig. 1c) and achieves a maximum for sample containing 20% La. Since this sample is comprised of two fluorite-like phases [15], this suggests that the oxygen transfer along disordered domain/interphase boundaries is also responsible for oxidation of activated CH_x fragments into deep oxidation products.

For the same matrix (Ce–Zr–O) and the same dopant content, variation of the specific rates of methane transformation into syngas with the nature of a dopant (La > Pr > Gd) follows the order of the sizes of respective Ln^{3+} cations: rLa^{3+}(1.17 Å) > Pr^{3+} (1.14 Å) > rGd^{3+} (1.053 Å) [39]. Apparently, in high-temperature reducing conditions of syngas generation, predominant part of Pr is in 3+ state, which justifies such a consideration. Since the size of doping cations affects the lattice

oxygen mobility in doped ceria–zirconia solid solution (vide supra), this suggests that the oxygen mobility in the lattice and, hence, in the surface layer of these supports determines a scale of the specific catalytic activity of supported Pt in POM. The same order was in general observed in specific rates of methane oxidation into combustion products (CO_2) for all three ceria–zirconia-based catalytic systems (Fig. 1c). For Pt on single-phase Ce–Zr–Gd (Pr) supports, monotonous decline of CO_2 formation rate with the dopant content agrees with the decrease of the lattice oxygen mobility caused by the local coordination polyhedra rearrangement eliminating anion vacancies. Nevertheless, both the rate of methane transformation and H_2 formation increase with the dopant content at $x > 10$ at.% reflecting mainly trend in variation of the Pt dispersion (vide supra).

For Pt supported onto doped ceria, the lowest activity was observed for Pr-doped samples, despite a rather high lattice oxygen mobility and Pt dispersion. This can be explained by the most oxidized state of supported Pt revealed by XPS [23,24], and, hence, a low ability to activate methane molecules. Apparently, this partially oxidized state of Pt is retained even in reducing reaction conditions due to a strong interaction with support.

For Pt on Gd-doped ceria, the rate of methane transformation is much higher correlating both with Pt dispersion and the lattice oxygen mobility (vide supra). However, in this case, methane is mainly transformed into deep oxidation products (Fig. 1c), so the specific rate of hydrogen generation is quite moderate (Fig. 1b). Hence, too high oxygen mobility and/or reactivity determined by the metal–oxygen bonding strength result in the combustion of activated CH_x fragments and CO/H_2 products.

For Pt/Sm-doped ceria, variation of the specific rates of methane transformation, H_2 and CO_2 formation with Sm content (Fig. 1) exactly follows the trend for the oxygen mobility (Fig. 4). The highest rates were achieved for a sample with a high (40%) Sm content (Fig. 1). For this sample, decoration of Pt clusters by SmO_x species ensures developed Pt–MeO_x boundary required for conjugation of the steps of CH_4 and oxidants activation. While oxygen mobility is apparently comparable for Gd-and Sm-doped ceria, a higher selectivity of methane transformation into syngas for the latter system seems to correlate with a higher basicity of a bigger Sm cation [39], which helps to increase the bonding strength of reactive oxygen species decreasing their combustion ability.

Comparison of the effect of the same doping cation (i.e. Pr) on the lattice oxygen mobility of different oxide matrix such as ceria or ceria–zirconia and state of supported Pt clearly reveals a great specificity apparently determined by the variation of the defect structure of nanocrystalline complex oxide systems as well as their surface properties affected by the dopant segregation and its dominating oxidation state [23,24].

3.5. Details of the reaction mechanism

Details of the reaction mechanism of methane selective oxidation into syngas at short contact times were elucidated for Pt/Ce–Zr–La sample (20% La) possessing the highest activity and selectivity among studied systems.

To estimate the rate constant of the oxygen transfer between the metal and support, SSITKA experiments with $^{18}O_2$ have been carried out. The typical results are shown in Fig. 7. In the absence of Pt the rate of isotope exchange is determined by interaction of gas phase oxygen with the active sites of support. After Pt addition, a faster pathway of the label transport appears through the spillover from Pt to the support followed by the surface diffusion. Promoting effect of platinum on the dynamics of the oxygen exchange, however, decreases as temperature rises up to the values typical for CH_4 selective oxidation to syngas: transient curves becomes closer thus suggesting important role of support properties in both high-temperature activity and syngas selectivity.

Modeling of the dynamics of isotope exchange gives estimations of the rate constants and activation energies for the steps of oxygen interaction with active sites of the support and Pt; coefficients and activation energies of oxygen surface and bulk diffusion were determined as well. The details of this modeling are beyond the scope of this paper and will be presented elsewhere [40]. Estimated constants of exchange, namely, $k_{support} = 0.13\ s^{-1}$ at 650 °C and 0.75 at 850 °C; $k_{Pt} = 15\ s^{-1}$ at 650 °C and $24\ s^{-1}$ at 850 °C, $K_{spill\text{-}over} = 15–20\ s^{-1}$, $D_{bulk} > 4 \times 10^{-13}\ cm^2/s$ (presumably, bulk diffusion occurs along domain boundaries), are rather close to those determined earlier by Dong et al. [41]. The value of the spill-over rate constant is comparable with that characterizing the oxygen

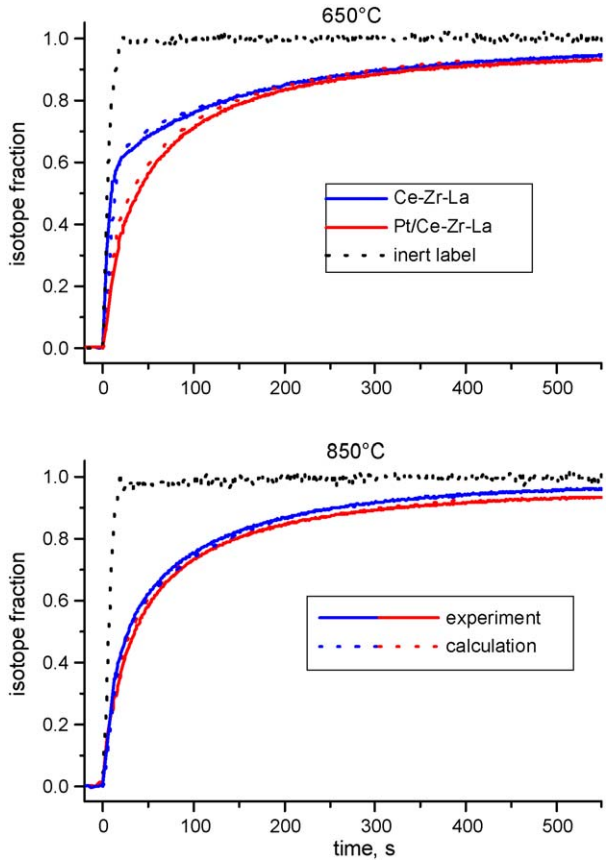

Fig. 7. Isotopic fractions of ^{18}O in O_2 compared to the Ne response vs. time upon switching from $^{16}O_2$ to $^{18}O_2$ in 2 vol.% O_2 in Ar flow for Ce–Zr–La–O based (20 at.% La) samples. Contact time 0.01 s.

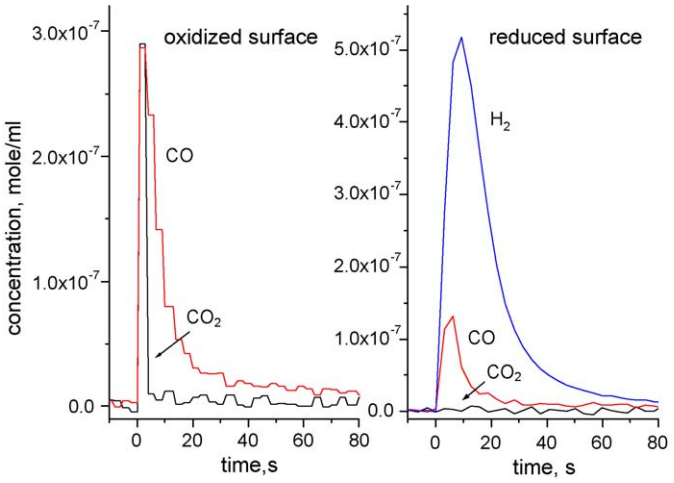

Fig. 8. Transient responses of CO, CO_2 and H_2 after switching from He to the reaction mixture 4.3% CH_4 in He over pre-oxidized or pre-reduced 1.4% Pt/CeO_2–ZrO_2–La_2O_3 sample at 650 °C.

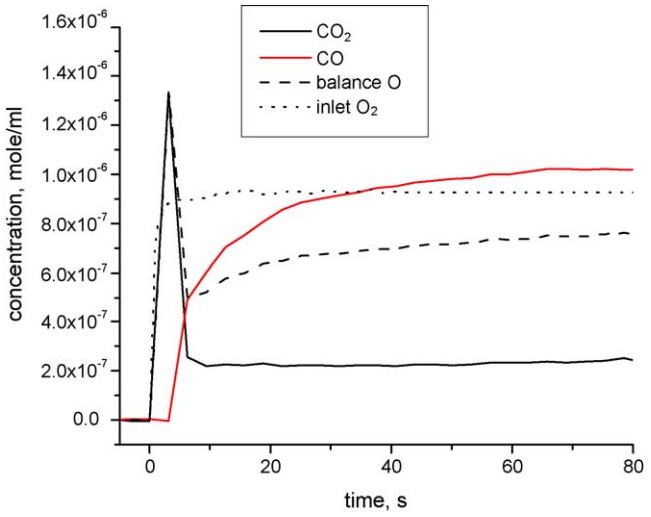

Fig. 9. Transient responses of CO, CO_2, oxygen (as O_2) incorporated into CO_x (balance O) as compared with oxygen at the reactor inlet (inlet O_2) after switching from He to the reaction mixture 4.3% CH_4 + 2.2% O_2 in He over pre-oxidized sample of 1.4% Pt/CeO_2–ZrO_2–La_2O_3. T = 650 °C.

exchange over Pt sites, thus implying that at least this stage is fast enough to be important for the overall reaction scheme.

Modeling the transients for Pt/Ce–Zr–La samples with $CH_4 + O_2$ and $CO + H_2O$ feeds with a due regard for existence of surface oxygen forms differing by reactivity allowed to ascertain the kinetic scheme of the reaction and estimate the rate constants of separate POM stages as well. Since the scope of this research including fitting transients to derive constants of the surface reactions certainly could not be reflected properly within a limited volume of this paper, all details and discussion will be given in a separate publication [42]. Here, only the most important features are illustrated and commented.

Thus, for oxidized Pt-containing sample, simultaneous appearance of both CO and CO_2 at stepwise switch from He to CH_4 suggests that CO is a primary product (Fig. 8), which agrees with the direct scheme of syngas generation from methane. For sample pre-reduced in hydrogen, efficient formation of syngas under sample contact with the feed containing methane without oxygen proves a rapid transfer of oxygen atoms from the bulk of oxide to the surface Pt clusters (Fig. 8). Similarly, in the presence of O_2 in the feed, the quantity of oxygen incorporated into the reaction products (CO and CO_2) in the first moment after the switch from He to $CH_4 + O_2$ mixture exceeds substantially that at the reactor inlet (Fig. 9). Complete absence of CO at the very beginning of the transient in the presence of oxygen in the feed over the oxidized catalyst is due to fast CO oxidation with numerous oxidized sites rapidly refilled by the gas-phase oxygen. In the absence of oxygen, these sites are fast depleted. As a consequence, CO_2 formation stops fast, while a delayed evolution of CO was observed.

Fitting transients with a due regard for occurrence of the water-gas shift reaction studied in separate experiments [42] allowed to estimate the rate constant of the oxygen spill-over from support to Pt found to be $\sim 50\ s^{-1}$. This value is rather close to the rate constants of stages leading to syngas generation such as (i) $CH_4 + Pt \rightarrow PtCH_x + H_2$ ($>100\ s^{-1}$) and (ii) PtO + $PtCH_x \rightarrow CO + Pt + H_2$ (H_2O) ($\sim 300\ s^{-1}$). Hence, the surface oxygen mobility is sufficiently high to avoid excessive accumulation of hydrocarbon radicals generated on Pt leading to coking. However, its rate constant is lower than the rate constant of stage (i), so some amount of hydrocarbon species will be accumulated on the Pt surface blocking sites for faster step of O_2 dissociation and thus preventing undesired excessive oxidation of Pt. This stage is also slower than the step of the radicals oxidation by the oxygen atoms supplied to Pt clusters boundary, so it could be indeed rate-determining in some conditions. Some depletion of the reactive oxygen species around Pt clusters might help to avoid excessive oxidation/combustion of CH_x radical species. At high operating temperatures (900–1000 °C), the surface hydroxylation and carboxylation is expected to be quite low, so the real transfer of oxygen atoms is apparently responsible for the methane selective oxidation. At moderate (600–700 °C) operating temperatures, hydroxyls or (hydroxo)carbonate species could participate in the CH_x fragments oxidation, so their transfer should be taken into account as well.

4. Conclusions

Systematic studies of the lattice oxygen mobility and reactivity in nanocrystalline fluorite-like supports based upon doped ceria or ceria–zirconia with supported Pt or without it in oxidized or reduced states revealed that variation of the type and content of a dopant as well as the oxide host matrix allows to broadly vary these parameters controlled at the microscopic level by the real/defect structure and Pt-support interaction. As the result, in majority of cases, a strong parallelism is observed between parameters characterizing the lattice oxygen mobility both for oxidized or partially reduced samples determined by using such techniques as oxygen isotope exchange or O_2 TPD, from one side, and H_2 TPR on the other side. Ability of Pt to activate methane correlates in general with its dispersion, though being negatively affected in some cases by too strong

Pt-support interaction leading to stabilization of oxidized Pt forms even in reaction conditions. Reasonable correlations were also observed between the oxygen mobility in supports and the specific rate of methane transformation in POM. At the same average lattice oxygen mobility, selectivity of methane transformation into syngas appears to be determined by the bonding strength of oxygen (or other oxygen-containing species such as hydroxyls, carbonates etc) as well, which reaches approximately the optimum value for such doping cations as La incorporated into the ceria–zirconia matrix or Sm incorporated into ceria lattice. This allows to ensure a high efficiency of methane transformation into syngas along with stability of these catalysts against coking. Direct estimation of the rate constants of the oxygen spill-over from the Pt to support and vice versa using kinetic transient and SSITKA techniques proved that indeed they are sufficiently high to prevent carbon accumulation on Pt. The results obtained within this study support the bifunctional scheme of methane transformation into syngas with the reaction occurring on the interface between the metal particle and support.

Acknowledgements

This work was in part supported by INTAS 01-2162, ISTC 2529 and RFBR – CNRS 05-03-34761_a Projects. Yu. Ivanova staying at the IRC (Lyon) to carry out SSITKA experiments was supported by the Grant of the Embassy of France in Russia.

References

[1] M. Krumpelt, S. Ahmed, R. Kumar, R. Doshi, US Patent 6,110,861 (2000).
[2] W. Wang, S.M. Stagg-Williams, F.B. Noronha, L.V. Mattos, F.B. Passos, Catal. Today 98 (2004) 553.
[3] D.A. Hickman, L.D. Schmidt, Science 259 (1993) 343.
[4] D.A. Hickman, L.D. Schmidt, J. Catal. 138 (1992) 267.
[5] M.C.J. Bradford, M.A. Vannice, J. Catal. 173 (1998) 157.
[6] M.M.V.M. Souza, M. Schmal, Appl. Catal. A: Gen. 255 (2003) 83.
[7] J. Kašpar, P. Fornasiero, Catalysis by ceria and related materials, in: A. Trovarelli (Ed.), Catalytic Science Series, vol. 2, Imperial College Press, London, UK, 2002, pp. 217–241.
[8] J. Wei, E. Iglesia, J. Phys. Chem. 108 (2004) 4094.
[9] J. Wei, E. Iglesia, J. Catal. 224 (2004) 370.
[10] J. Wei, E. Iglesia, J. Catal. 225 (2004) 116.
[11] E. Odier, Y. Schuurman, K. Barral, C. Mirodatos, Stud. Surf. Sci. Catal. 147 (2004) 79.
[12] M. Fathi, F. Monnet, Y. Schuurman, A. Holmen, C. Mirodatos, J. Catal. 190 (2000) 439.
[13] A. Bourane, D. Bianchi, J. Catal. 218 (2003) 447.
[14] V.A. Sadykov, T.G. Kuznetsova, G.M. Alikina, Y.V. Frolova, A.I. Lukashevich, Y.V. Potapova, V.S. Muzykantov, V.A. Rogov, V.V. Kriventsov, D.I. Kochubei, E.M. Moroz, D.I. Zyuzin, V.I. Zaikovskii, V.N. Kolomiichuk, E.A. Paukshtis, E.B. Burgina, V.V. Zyryanov, N.F. Uvarov, S. Neophytides, E. Kemnitz, Catal. Today 93–95 (2004) 45.
[15] T.G. Kuznetsova, V.A. Sadykov, E.M. Moroz, S.N. Trukhan, E.A. Paukshtis, V.N. Kolomiichuk, E.B. Burgina, V.I. Zaikovskii, M.A. Fedotov, V.V. Lunin, E. Kemnitz, Stud. Surf. Sci. Catal. 143 (2002) 659.
[16] V.A. Sadykov, Yu.V. Frolova, V.V. Kriventsov, D.I. Kochubei, E.M. Moroz, D.A. Zyuzin, Yu.V. Potapova, V.S. Muzykantov, V.I. Zaikovskii, E.B. Burgina, V.P. Ivanov, H. Borchert, S. Neophytides, E. Kemnitz, K. Scheurell, Mater. Res. Soc. Symp. Proc. 835 (2005) 199.
[17] V.A. Sadykov, V.I. Voronin, A.N. Petrov, Yu.V. Frolova, V.V. Kriventsov, D.I. Kochubei, V.I. Zaikovskii, H. Borchert, S. Neophytides, Mater. Res. Soc. Symp. Proc. 835 (2005) 205.
[18] V.A. Sadykov, Yu.V. Frolova, G.M. Alikina, A.I. Lukashevich, V.S. Muzykantov, V.A. Rogov, E.M. Moroz, D.A. Zyuzin, V.P. Ivanov, H. Borchert, E.A. Paukshtis, V.I. Bukhtiyarov, V.V. Kaichev, S. Neophytides, E. Kemnitz, K. Scheurell, React. Kinet. Catal. Lett. 86 (2005) 21.
[19] V.A. Sadykov, Yu.V. Frolova, G.M. Alikina, A.I. Lukashevich, S. Neophytides, React. Kinet. Catal. Lett. 86 (2005) 29.
[20] V.A. Sadykov, S.N. Pavlova, R.V. Bunina, G.M. Alikina, S.F. Tikhov, T.G. Kuznetsova, Yu.V. Frolova, A.I. Lukashevich, O.I. Snegurenko, N.N. Sazonova, E.V. Kazantseva, Yu.N. Dyatlova, V.V. Usol'tsev, I.A. Zolotarskii, L.N. Bobrova, V.A. Kuz'min, L.L. Gogin, Z.Yu. Vostrikov, Yu.V. Potapova, V.S. Muzykantov, E.A. Paukshtis, E.B. Burgina, V.A. Rogov, V.A. Sobyanin, V.N. Parmon, Kinet. Catal. 46 (2005) 227.
[21] V.A. Sadykov, Yu.V. Frolova, G.M. Alikina, A.I. Lukashevich, V.S. Muzykantov, V.A. Rogov, E.M. Moroz, D.A. Zyuzin, V.P. Ivanov, H. Borchert, E.A. Paukshtis, V.I. Bukhtiyarov, V.V. Kaichev, S. Neophytides, E. Kemnitz, K. Scheurell, React. Kinet. Catal. Lett. 85 (2005) 367.
[22] V.A. Sadykov, Yu.V. Frolova, G.M. Alikina, A.I. Lukashevich, S. Neophytides, React Kinet. Catal. Lett. 85 (2005) 375.
[23] H. Borchert, Yu.V. Frolova, V.V. Kaichev, I.P. Prosvirin, G.M. Alikina, A.I. Lukashevich, V.I. Zaikovskii, E.M. Moroz, S.N. Trukhan, V.P. Ivanov, E.A. Paukshtis, V.I. Bukhtiyarov, V.A. Sadykov, J. Phys. Chem. B 109 (2005) 5728.
[24] H. Borchert, Yu. Borchert, V.V. Kaichev, I.P. Prosvirin, G.M. Alikina, A.I. Lukashevich, V.I. Zaikovskii, E.M. Moroz, E.A. Paukshtis, V.I. Bukhtiyarov, V.A. Sadykov, J. Phys. Chem. B. 109 (2005) 20077.
[25] V.A. Sadykov, Yu. Borchert, N.V. Mezentseva, G.M. Alikina, A.I. Lukashevich, E.A. Paukshtis, V.S. Muzykantov, L.Ch. Batuev, T.G. Kuznetsova, E.M. Moroz, D.A. Zyuzin, V.P. Kol'ko, E.B. Burgina, V.V. Kriventsov, D.I. Kochubei, E. Kemnitz, K. Scheurell, Mater. Res. Soc. Symp. Proc. 900E (2006) O10.4.
[26] E. Kemnitz, A.A. Galkin, T. Olesch, S. Scheurell, A.P. Mozhaev, G.N. Mazo, J. Therm. Anal. 48 (1997) 997.
[27] V.S. Muzykantov, E. Kemnitz, V.A. Sadykov, V.V. Lunin, Kinetika I Kataliz 44 (2003) 349 (in Russian).
[28] E. Mamontov, T. Egami, R. Brezny, M. Koranne, S. Tagy, J Phys. Chem. B 104 (2000) 11110.
[29] M. Boaro, A. Trovarelli, J.-H. Hwang, T.O. Mason, Solid State Ionics 147 (2002) 85.
[30] N.N. Bulgakov, V.A. Sadykov, V.V. Lunin, E. Kemnitz, React. Kinet. Catal. Lett. 76 (2002) 103.
[31] M. Pirzada, R.W. Grimes, L. Minervini, J.F. Maguire, K.E. Sickafus, Solid State Ionics 140 (2001) 201.
[32] Zh. Hui, G. Nicolas, V. Francoise, P. Michele, Solid State Ionics 140 (2001) 201.
[33] A. Tsoga, A. Naoumidis, D. Syoever, Solid State Ionics 135 (2000) 403.
[34] H. Yamamura, H. Nishino, K. Kakinuma, K. Nomura, Solid State Ionics 158 (2003) 359.
[35] C. Descorme, Y. Madier, D. Duprez, J. Catal. 196 (2000) 167.
[36] A. Iglesias-Juez, A. Martinez-Arias, M. Fernandes-Garcia, J. Catal. 221 (2004) 148.
[37] M.S. Brogan, T.J. Dines, J.A. Cairns, J. Chem. Soc. Farad. Trans. 90 (1994) 1461.
[38] Y.-F. Yao, Ind. Eng. Chem. Prod. Res. Dev. 19 (1980) 293.
[39] R.D. Shannon, Acta Crystallogr. A 32 (1976) 751.
[40] Yu. Ivanova, K. Sadovskaya, L. Pinaeva, C. Mirodatos, A. van Veen, V. Sadykov, T. Kuznetsova, J. Catal., 2006, submitted for publication.
[41] F. Dong, A. Suda, T. Tanabe, Y. Nagai, H. Sobukawa, H. Shinjoh, M. Sugiura, C. Descorme, D. Duprez, Catal. Today 93–95 (2004) 827.
[42] L.G. Pinaeva, Yu.A. Ivanova, E.M. Sadovskaya, T.G. Kuznetsova, V.A. Sadykov, G. Grasso, Y. Schuurman, A.C. van Veen, C. Mirodatos, J. Catal., 2006, submitted for publication.